Analytical Study of Tessellated Structural-Architectural Reinforced Concrete Shear Walls

- 2 Mohammad Syed¹; Mohammad Moeini²; Pinar Okumus³; Negar Elhami Khorasani⁴; Brandon E. Ross⁵
- 3 and Michael Carlos Barrios Kleiss⁶
- 4 ¹Graduate Research Assistant, Dept. of Civil, Structural, and Environmental Engineering, Univ. at Buffalo, Buffalo,
- 5 NY 14260 (corresponding author). Email: s54@buffalo.edu
- 6 ²Graduate Research Assistant, Dept. of Architectural Engineering, The Pennsylvania State University, 104
- 7 Engineering Unit A, University Park, PA 16802. Email: mbm6448@psu.edu
- 8 ³Associate Professor, Dept. of Civil, Structural, and Environmental Engineering, Univ. at Buffalo, 222 Ketter Hall,
- 9 Buffalo, NY 14260. Email: pinaroku@buffalo.edu
- ⁴Assistant Professor, Dept. of Civil, Structural, and Environmental Engineering, Univ. at Buffalo, 136 Ketter Hall,
- 11 Buffalo, NY 14260. Email: negarkho@buffalo.edu
- ⁵Cottingham Associate Professor, Glenn Dept. of Civil Engineering, Clemson Univ., 109 Lowry Hall, Clemson, SC
- 13 *29634-0911. Email: bross2@clemson.edu*
- ⁶Associate Professor of Architecture, Structures & Computation & Watt Family Innovation Center Faculty Fellow,
- 15 School of Architecture, Clemson Univ., Lee Hall 3-123, Clemson, SC 29634-0911. Email: crbh@clemson.edu
- 16 DOI: https://doi.org/10.1016/i.engstruct.2021.112768

17 Abstract

- 18 This paper studies the lateral behavior of a reinforced concrete tessellated structural-architectural (TeSA)
- shear wall system. TeSA walls are made of prefabricated repetitive tiles and have the ability to localize
- damage which occurs under extreme loading. A TeSA wall is intended for architectural interest, automated
- 21 construction, reconfiguration, disassembly, and reuse. This study focuses on TeSA tiles that are
- 22 topologically interlocking in two directions. Nonlinear finite element analysis is used to study the
- 23 monotonic pushover behavior of TeSA walls with different edge tile configurations and a comparison is
- 24 made thereof with a conventional reinforced concrete shear wall. The results indicate that the strength of
- 25 TeSA walls is not significantly affected by the configuration of edge tiles. Damage progression in tiles and
- 26 the number of damaged tiles that need to be replaced are also presented at different drift ratios. The study
- shows that reinforcement ratio substantially affects the wall lateral capacity. Finally, a simplified cross-
- 28 sectional analysis procedure is proposed to provide a lower and upper bound estimate of the lateral capacity
- of TeSA walls.
- 30 **Keywords:** Shear wall, Resiliency, Modular construction, Prefabrication, Tessellation, Finite element
- 31 analysis.

1. Introduction

32

33

34

35

36

37

38

39

40

41

42

43

44

45

46

47

48

49

50

51

52

53

54

55

56

This paper characterizes the structural behavior of a new type of reinforced concrete (RC) shear wall that is composed of tessellated tiles. Structural shear walls are widely used as the primary system to resist lateral forces induced by earthquakes and wind. Well-detailed RC shear walls provide adequate stiffness, strength, and ductility to meet demands of extreme events such as earthquakes [1, 2]. One of the major disadvantages of conventional RC shear walls, which motivated this research, is the difficulty to repair damage from extreme loading. RC shear walls have bonded reinforcement for lateral force resistance, which results in rapid crack growth with increasing drift ratios. Prefabricated rocking concrete systems have been proposed to avoid damage in structural walls [3-12]. Damage Avoidance Design philosophy, in which damage is avoided by special connection detailing, was first introduced by Mander and Cheng [3] and later adopted by others for precast and rocking RC shear walls [9, 10]. More information on conventional RC shear wall behavior can be found elsewhere [13, 14]. This paper discusses the structural behavior of a new tessellated structural-architectural (TeSA) wall system [15] made of repetitive pattern of tiles (tessellations) under lateral loading. Composed of discontinuous precast elements, TeSA walls are intended to enable fast repair and recovery from extreme events, damage localization, fast and automated construction and easy reconfiguration. The objective of this paper is to characterize the structural performance of TeSA walls through finite element analysis (FEA). FE models of the TeSA wall and an equivalent conventional wall, for which test data were available, are prepared and their results are compared. Damage propagation within TeSA wall system is studied. Multiple TeSA configurations are investigated and a simplified, section-analysis based capacity-prediction approach is proposed. Edge treatments are an important consideration in tessellated patterns, and the impact of edge tile configurations is given particular attention in the analyses.

2. TeSA – Concept and Application as a Structural System

A tessellation is a repetitive arrangement of interchangeable tiles that geometrically cover a surface without overlaps or openings. There are many examples of tessellations in architecture [16], e.g., the Arab World

Institute in Paris and Al Bahar Towers in Abu Dhabi have tessellated façades for environmental control. However, tessellated members have seen limited use as parts of building structural systems [15]. The TeSA walls have the potential to serve as the lateral load resisting system in a building while providing an aesthetically pleasing design solution. This new concept is in its development stage, and has to be thoroughly analyzed and experimentally tested before it can be applied in practice. TeSA walls open up possibilities for various tile patterns and interlocking systems, each of which requires investigation. In addition, once tested at the laboratory scale, the construction procedure and repair methods should be outlined. The TeSA walls are not intended to replace RC walls in all applications, especially for cases with high seismic demands. Instead, they provide an alternative design solution where the shear demand can be met and when there is interest in TeSA systems' benefits in reparability and aesthetic appeal. A hybrid system comprising TeSA walls and conventional RC walls could also be an option. As part of a long-term objective to develop a new structural system, this paper investigates the structural behavior of RC TeSA shear walls with tiles that topologically interlock in two directions (2-D interlocking) as shown in Fig. 1. In a 2-D topologically interlocking tessellation, separation of tiles is prevented by contact in two directions through interlocking of neighboring tiles.

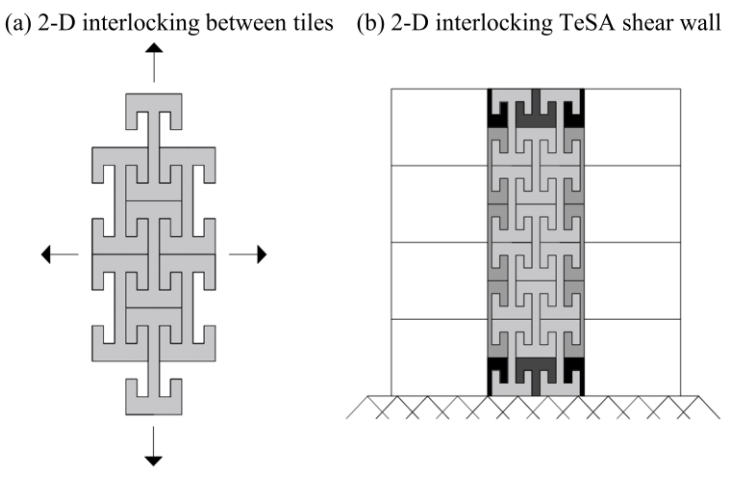


Fig. 1. 2-D interlocking tiles in a TeSA shear wall

One potential advantage of TeSA structures over conventional, solid structures, is their damage tolerance.

Cracking in a TeSA tile may be interrupted once it reaches a free edge, localizing in a single tile rather than

- propagating across a solid structure. This phenomena has been shown in experiments at scales much smaller than that of civil engineering structures [17, 18]. Similarly, ability to replace individual tiles enables reparability and reuse. Mather et al. [19] showed that at material scale, the material can be remanufactured and replaced with minimal performance loss. Ross et.al [15] provides a detailed discussion on the concept, likely benefits and future opportunities of TeSA systems.
- Previous research on topologically-interlocked elements has primarily focused on small-scale structures [20-22]. The current research studies the structural characterization of TeSA shear walls at building scale for potential use as lateral load-resisting systems.

3. FEA Methods and Validation

FEA is used to characterize structural response and capacity of TeSA walls. The FE model is validated using experimental data from a conventional shear wall (specimen RW2) tested by Thomsen and Wallace [23] under lateral cyclic loading. Details such as FE formulation and material models, from the conventional wall are then applied to similarly sized TeSA wall. A commercial FEA software Abaqus [24] is used. The conventional wall is $3600 \, \text{mm} \, (141.7 \, \text{in.})$ high and $1200 \, \text{mm} \, (47.2 \, \text{in.})$ wide. The cross section is rectangular with boundary elements confined using steel ties (4.76 mm or 3/16 in. diameter) with spacing of 50 mm (2.0 in.). Each boundary element has two layers of $\phi 10$ (No. 3) vertical bars on each face of the wall with spacing of 50 mm (2.0 in.). The web of the wall (away from the boundaries) is reinforced with two layers of $\phi 6$ (No. 2) vertical and horizontal bars on each face, spaced at 190 mm (7.5 in.) on center. The clear cover is 9 mm (0.35 in.). The elevation and reinforcement details of the specimen are shown in Fig. 2.

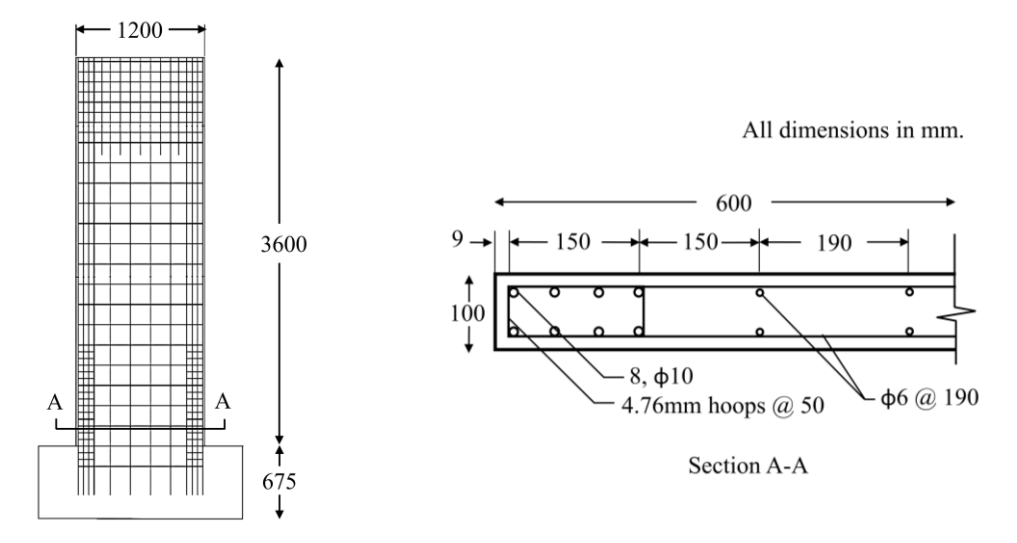


Fig. 2. Elevation and reinforcement details of specimen - adapted from Thomsen and Wallace [23]

3.1 Material properties

Reinforcing steel stress-strain curves provided by Thomsen and Wallace [25], shown in Fig. 3, are used for generating material-model inputs for reinforcement. All reinforcing steel in the conventional and TeSA walls, has a specified yield stress of 414 MPa (Grade 60 steel).

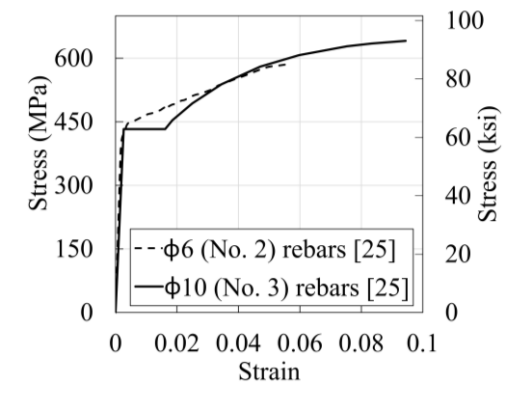


Fig. 3. Steel stress-strain curves - adapted from Thomsen and Wallace [25]

Concrete material for foundation and cap material are modeled using linear-elastic properties. Nonlinear-inelastic properties are used for the wall. Nonlinear-inelastic response is defined using the "concrete damaged plasticity (CDP)" model of Abaqus, which uses isotropic hardening and non-associated plastic flow rule. The model uses the yield function developed by Lubliner et al. [26], and Lee and Fenves [27]. The CDP model requires defining the plasticity parameters, which are typically not measured in testing and

108

109

110

111

112

113

114

115

116

117

118

119

120

121

122

123

124

125

126

127

128

129

130

131

were not reported by Thomsen and Wallace [23]. These parameters include eccentricity (ϵ), the biaxial-touniaxial compressive stress ratio (f_{h0}/f_{c0}) , and tensile-to-compressive meridian stress ratio (K_c). The parameter eccentricity (ϵ) defines the rate at which the flow potential becomes asymptotic. A value of 0.1 (considered herein) denotes nearly constant dilation angle over range of confining pressures. The ratios f_{b0}/f_{c0} and K_c are taken as the default values in Abaqus [24] as 1.16 and 0.667, respectively, which are comparable to those proposed by Lim et al. [28]. The dilation angle (ψ) is taken as 31 degrees. The response was insensitive to the dilation angle when the angle was varied between 25 degrees and 40 degrees. Moreover, the value is well within the range suggested by Wosatko et al. [29]. Poisson's ratio of concrete is taken as 0.2 per fib Model Code 2010 [30]. The modulus of elasticity of concrete in compression and tension is taken as 27.7 GPa (4026 ksi). Modulus of elasticity was calculated as the secant modulus at 40% of the peak compressive stress [30] on the concrete stress-strain curve in compression obtained from test data. The CDP model also requires defining concrete behavior in compression and tension. For concrete in compression, stress-strain relationship between 40% and 100% of peak stress is defined as obtained from cylinder test data. Cylinder test data are available only up to peak strength. For post-peak behavior of concrete in compression, the *fib* Model Code 2010 [30] constitutive relationship is assumed. For concrete in tension, the pre-cracking behavior is modeled as elastic with the same modulus of elasticity as that for compression up to the tensile strength of concrete (f_i) of 3.7 MPa (0.54 ksi), calculated per section 5.1.5.1 of fib Model Code 2010 [30]. Concrete behavior in tension after cracking is defined using fracture energy cracking criterion described by bilinear stress and crack-opening (displacement) relationship per fib Model Code 2010 [30]. In this model, post-cracking behavior depends on the fracture energy of concrete, i.e., the energy required to generate a tensile crack of unit area. Based on the available compression strength test data, the value of fracture energy (G_f) is calculated as 144 N/m (9.8 lb/ft) per fib Model Code 2010 section 5.1.5.2 [30]. The same modulus of elasticity defined for the wall is used for the linear-elastic model

of the foundation and the modulus of elasticity of steel is used for the linear-elastic model of the cap beam.

The constitutive relationships for concrete in compression and tension are shown in Fig. 4.

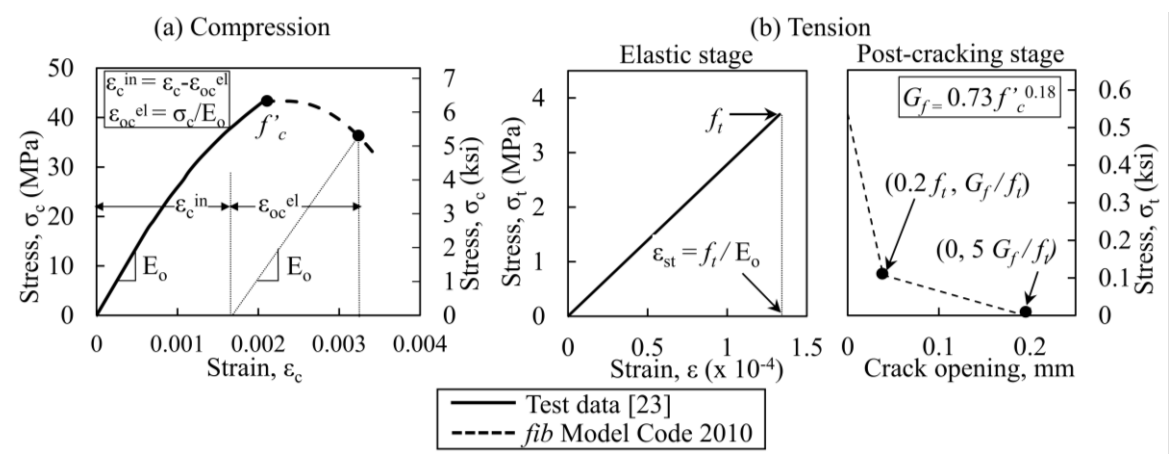


Fig. 4. Concrete stress-strain relationship used in the FE model

3.2 Finite Elements

Eight-node brick elements with reduced integration and hourglass control (C3D8R in Abaqus) and with size of 25mm×25mm×25mm (1in.×1in.×1in.) are used to model concrete wall elements. The mesh size was selected so that there were multiple finite elements across thickness of all tiles and that the results were not sensitive to the mesh size. To model reinforcement bars, two-node 3-D truss elements (T3D2 in Abaqus) are employed. Reinforcement bars are embedded inside concrete elements assuming perfect bond to concrete. Fig. 5 shows the mesh and an overall schematic of the model. Conventional and TeSA walls had the same mesh as shown in Fig. 5.

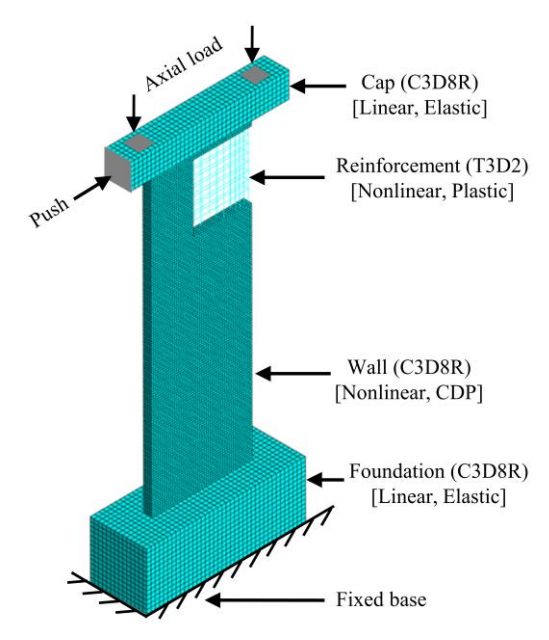


Fig. 5. Schematic of the FE model for the conventional wall

3.3 Boundary Conditions, Loading, and Solution Method

The wall is fixed at the base of the foundation. Sliding along wall-foundation interface or rebar buckling have not been considered in the current study. For TeSA walls, tiles at the base of the wall are tied to the foundation to prevent gap openings between the lowest set of tiles and foundation. An axial load of 378 kN (85 kips) or $0.07f_c'A_g$ is exerted on the wall through the cap beam, as shown in Fig. 5 (as applied during testing), where f_c' and A_g are the concrete compression strength and gross wall cross-section area, respectively. After axial load is applied, a gradually increasing lateral displacement is imposed on the cap beam on its side face. Walls are analyzed using static-general procedure with direct integration approach.

3.4 Model Validation for the Conventional Shear Wall

Fig. 6 compares lateral load-drift relationship from test data reported by Thomsen and Wallace [23] and from the FEA for the conventional shear wall. The FEA results correlate reasonably well with the test data, with a slight mismatch for initial stiffness, which can be challenging to capture as concrete cracks due to shrinkage before testing, strain penetration to foundation, and deformations within test fixtures may occur in testing. In addition, the experimental data used for the backbone curve pertains to cyclic test, which is subject to a higher loss of stiffness with increasing displacement amplitudes. Finally, inherent variabilities

in material properties, particularly of concrete, contribute to deviations between model and test results. The ultimate lateral load capacity predicted by the model is within 3% of the measured value reported after testing.

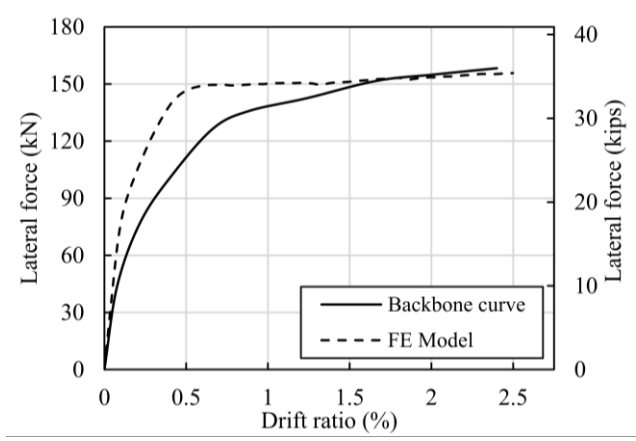


Fig. 6. Comparison of backbone (test-data) and pushover (FE model) curves for conventional shear wall

4. Description of the TeSA walls

The TeSA walls, studied in this paper, have the same outer dimensions and material properties as the conventional shear wall tested by Thomsen and Wallace [23]. The edge tiles, which refer to the single layer of tiles at the outermost edge of the wall across its height, may affect the lateral load capacity of the wall because of joint discontinuities. To assess the sensitivity of the TeSA walls to edge tile configuration, the following four TeSA walls with different edge tile patterns are introduced and investigated (Fig. 7):

- 1. Noncontinuous edge tile pattern
- 2. Continuous edge tile pattern
- 3. Staggered edge tile pattern A
- 4. Staggered edge tile pattern B

TeSA walls with staggered edge tiles have two layers of edge tiles across the wall thickness with staggered joints (overlapped tiles) across the wall height to contain gap openings between tiles when subjected to lateral load. When a gap opens up at one face of the wall, tiles at the other face restrain it. Edge tiles with

staggered pattern A are designed to provide more continuity compared to ones with staggered pattern B.

On the other hand, staggered pattern B edge tiles are smaller and therefore are easier to replace if damaged.

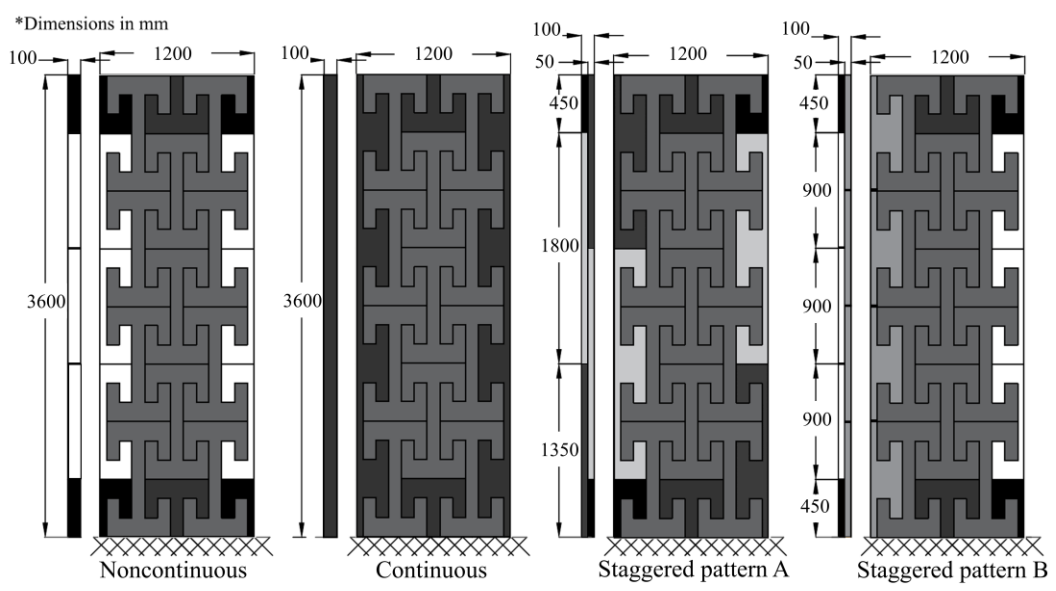


Fig. 7. TeSA wall configurations based on the edge tile pattern

Eight tile shapes, in total, are designed to construct the walls with different edge patterns, namely: Full tiles, C tiles, T tiles, Quarter (Q) tiles, QQ tiles, CQ tiles, CC tiles, and the continuous edge tile. The width and height of a Full tile (shown in Fig. 8) are set to 500 mm (19.7 in.) and 900 mm (35.4 in.) respectively. The other tiles are created from the Full tile, by cutting the height in half (T tile), the width in half (C tile) or both (Q tile).

The reinforcement of the bottom tiles continues into the foundation. This can be achieved by casting the bottom tiles with the foundation, by means of mechanical couplers or grouted ducts that house reinforcing bars for making reinforcement continuous across the foundation-tile interface.

The conventional wall that is used for comparison [23] and the tiles of the TeSA walls have the same longitudinal reinforcement ratio (1.2%), except for staggered edge tiles, where the ratio is double because the tile thickness is halved. The transverse reinforcement ratio for the conventional wall (0.32%), if adopted for the TeSA wall, results in unreasonably large spacing and low number of transverse rebars, which are not practical, particularly in the "extension" of flanges, where substantial shear is expected. The transverse reinforcement ratio is thus selected as 1.1%, except for the staggered edge tiles where the ratio is nearly

double because of the smaller thickness of edge tiles. The reinforcement detail of a Full tile is shown in

Fig. 6. Comparable reinforcement configurations are also used in the other tile shapes.

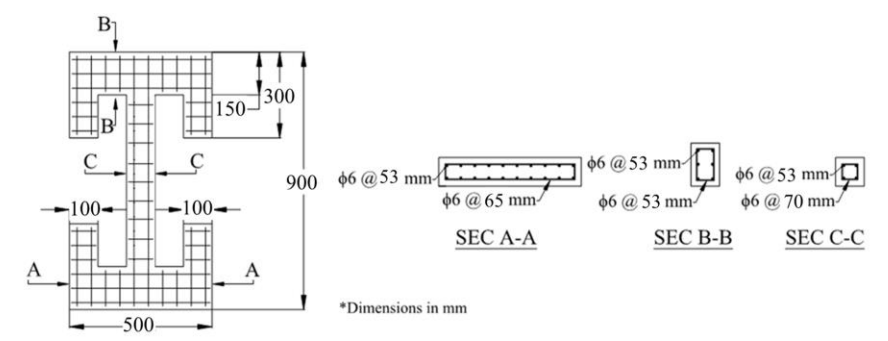


Fig. 8. Elevation, dimensions and cross section reinforcement details of the Full tile

In modeling the TeSA walls, contact between tiles is characterized using normal, hard contact behavior, which allows separation after contact (i.e., no penetration and no transfer of tensile stresses across contacting pieces), and tangential behavior with friction penalty. The friction coefficient is set to the lower-bound value of 0.6 per ACI 318-14 [31], which corresponds to "concrete pieces placed on hardened concrete with clean surface, free of laitance, and not intentionally roughened".

5. Results of TeSA Wall Analyses

198

199 200

201

202

203

204

205

206

- 5.1 Relationship of Lateral Load and Displacement
- Fig. 9 shows the load-deformation responses obtained from FEA for the conventional wall and the four
- 209 TeSA wall configurations of Fig. 7. Different TeSA walls exhibit comparable strength and initial stiffness,
- with staggered pattern A giving slightly higher peak strength than the rest.

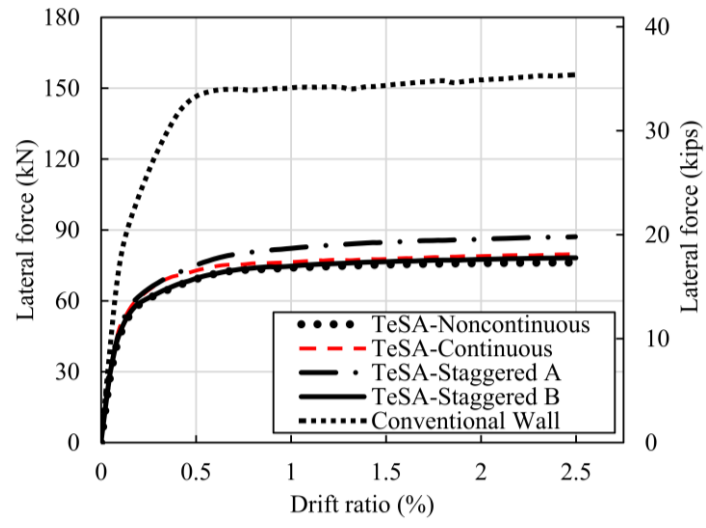


Fig. 9. Load deformation comparison of the conventional and TeSA walls

211 212

213

214

215

216

217

218

219

220

221

222

223

224

225

226

227

228

The peak strengths of TeSA walls with noncontinuous, continuous, staggered pattern A and staggered pattern B edge tiles are 49%, 51%, 56% and 50% of that of the conventional wall respectively, whereas the initial stiffness is 72%, 73%, 73% and 76% of the conventional wall, respectively. For a consistent comparison, the secant stiffness corresponding to 30% of the peak force value for each wall is reported as the initial stiffness, as the walls are not expected to undergo significant plastic deformations at this load. The results show that edge tile configuration has minimal impact on the lateral load capacity of the TeSA walls. Although the noncontinuous, continuous, and staggered B configurations lead to similar strengths, the latter provides better gap control owing to the presence of restraining tiles at all possible critical sections, which is not the case with the former two. Staggered A configuration has slightly higher strength than staggered B configuration due to taller overlapped edge tiles. Taller edge tiles may be harder to repair or replace in the event of damage. The load-displacement curves of the TeSA walls flatten because of gap openings and subsequently by the yielding of tile reinforcement. TeSA walls with different edge tile configurations have smaller capacities as compared to the equivalent conventional wall. Additional reinforcement, larger shear wall dimensions or additional shear walls may be required to obtain comparable capacities, although the architectural benefits offered by TeSA walls may offset the resulting additional costs.

5.2 Principal Strain Contours

229

230

231

232

233

234

235

236

237

238

239

240

241

242

243

244

245

246

247

248

249

250

251

Two different criteria are considered to study damage in the TeSA walls: concrete cracking and concrete crushing. Cracking strain of concrete is calculated as 1.33×10^{-4} by dividing its tensile strength, f_t [3.7] MPa (0.54 ksi)] by the modulus of elasticity, E₀ [27.7 GPa (4026 ksi)]. The crushing strain of unconfined concrete is taken as 0.0035 per fib Model Code 2010 [30] and was used as the unconfined concrete strain threshold in defining crushing damage. For the confined concrete cores in tiles, the compression strain at "failure", for which confined compressive stress becomes zero, was determined as 0.0200 per the constitutive model proposed by Mander et al. [32], and Karthik and Mander [33]. This strain was used as the confined concrete threshold in defining crushing damage. Fig. 10 and Fig. 11 show the principal tensile strains (indicator of concrete cracking) and principal compressive strains (indicator of concrete crushing) at 1.0% drift ratio, respectively. In these figures, gray and black colors indicate strains larger in magnitude than the calculated cracking strain (1.33×10^{-4}) and unconfined concrete crushing strain (3.5×10^{-3}) , respectively. Looking at the contour plots, there are discontinuous regions of cracked and crushed elements (grey and black colors) between neighboring tiles. This may be an indication of localization of cracking and crushing within discrete tile elements. Edge tile configuration tends to affect the damage pattern. TeSA walls with continuous and staggered pattern A configurations experience more cracking damage in the edge tiles due to their continuity across wall height. Any damage observed in continuous and staggered A edge tiles renders the entire edge tile unusable or warrants repair. The TeSA wall with noncontinuous edge tiles has similar damage behavior as staggered B configuration, while the latter better controls gap opening due to overlapping edge tiles across the height. The TeSA wall with staggered pattern B configuration is thus selected for further studies in this paper because of comparable strength of this wall to others, greater redundancy, better gap control and smaller edge tiles that facilitate easy replacement and repair in the event of damage.

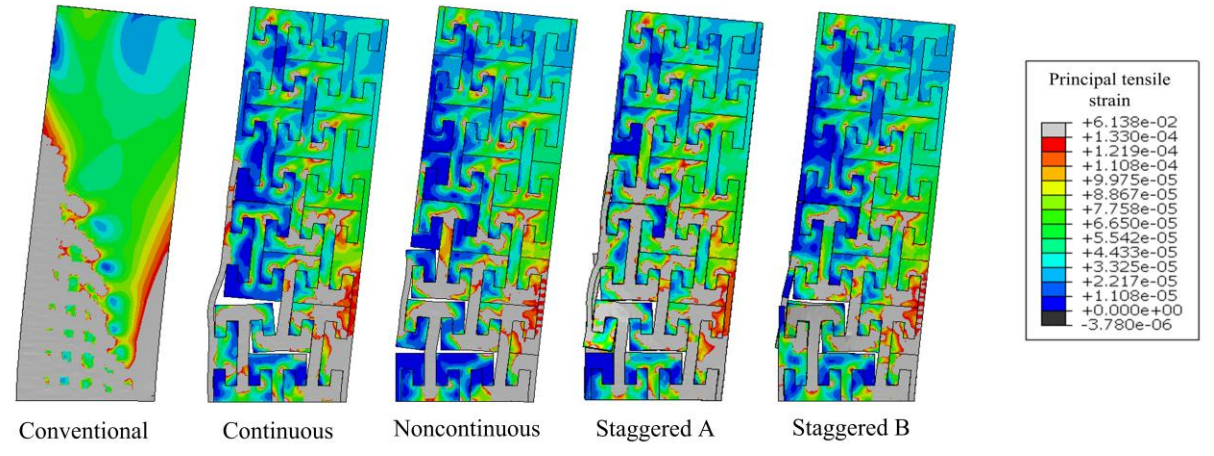


Fig. 10. Contour plots of principal tensile strain (cracking) at 1.0% drift ratio

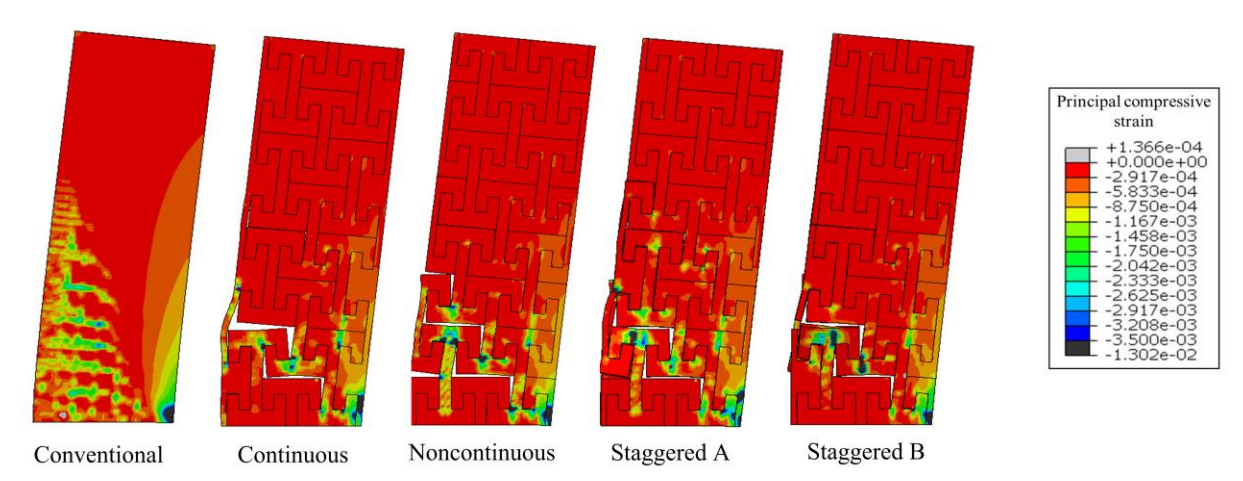


Fig. 11. Contour plots of principal compressive strain (crushing) at 1.0% drift ratio

6. Damage Quantification of TeSA Walls

6.1 Damage Evaluation at Wall Level

In this section, damage is evaluated more closely for the TeSA wall with staggered pattern B edge tiles. Using the cracking and crushing criteria established in the previous section, the percentage of finite elements that are crushed or cracked are compared for the conventional and the TeSA wall with the staggered edge tile pattern B. A finite element is considered cracked or crushed if its strain is above the cracking or crushing limit, respectively. Unconfined concrete ultimate compression strain (0.0035) is used to define the crushing limit.

It can be observed from Fig. 12 (a) that the percentage of cracked finite elements in the TeSA wall is significantly lower relative to the conventional wall at all drift ratios. The percentage of cracked finite elements at 2.5% drift ratio for the TeSA wall is 18.6%, whereas it is 27.1% for the conventional wall. Fig. 12 (b) shows that element crushing for both the conventional wall and TeSA wall begins at nearly 0.5% drift ratio and is more severe for the conventional wall at higher drift ratios. At around 1.5% drift ratio, a sharp increase in the percentage of crushed elements is observed for the conventional wall, while crushing in the TeSA wall maintains a constant rate. The number of crushed elements of the TeSA wall with staggered edge tile pattern B is 37% of that of the conventional wall at 2.5% drift.

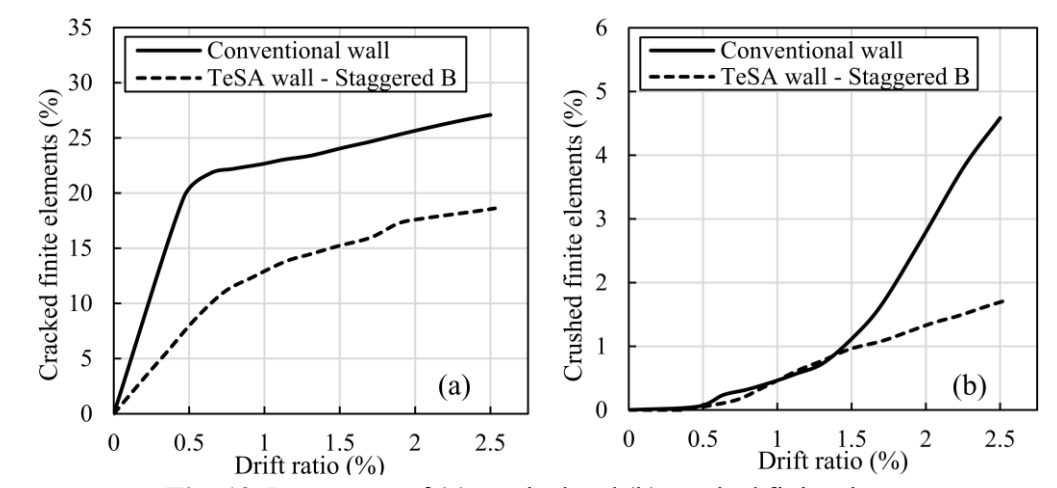


Fig. 12. Percentage of (a) cracked and (b) crushed finite elements

6.2 Damage Evaluation at Tile Level

The defined crushing and cracking criteria are also used to investigate damage in each individual tile for the TeSA wall with staggered edge tile pattern B. If more than 20% of the elements of an individual tile have strains greater than the limiting cracking strain, the tile is considered damaged in tension. A tile is considered damaged in compression, if any element (more than 0% of the elements) in a tile has strains above the threshold concrete strains established earlier. For comparison, both confined and unconfined concrete strain thresholds have been considered. Sensitivity of the number of damaged tiles to the defined damage thresholds is also studied in this section.

In Fig. 13, the tiles that are damaged due to cracking per the aforementioned criterion are indicated by shading and hatching for salient drift ratios. It should be noted that the front and back faces of the TeSA wall have different edge tiles, as the edge tiles are staggered (refer to pattern B in Fig. 7). Tiles undergo cracking damage relatively early and the number of cracked tiles increases with increasing lateral displacement. At drift ratio of 1.0%, 8 out of 31 tiles would require repair or replacement due to damage caused by cracking. The number of cracked tiles increases till 2.5% drift ratio, with the maximum number of tiles damaged being 12.

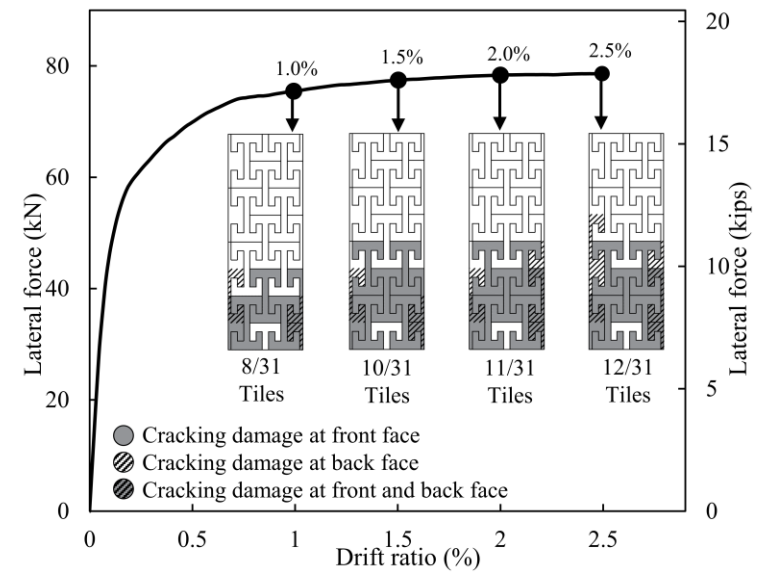


Fig. 13. Damaged tiles due to cracking at varying drift ratios

Similarly, Fig. 14 shows the tiles that are considered damaged under compression on the front and back faces of the wall as hatched or shaded. When unconfined concrete strain limit is considered to define damage, 7 to 10 tiles experience crushing for drift ratios ranging between 1.0% and 2.5%. Tiles near the base of the wall, within the first two rows of Full tiles from the base, are the first to experience crushing damage. Additional tiles get crushed within the first and second row of Full tiles from the base with increasing drift ratios, eventually resulting in 10 crushed tiles at 2.5% drift ratio. If confined concrete strain limit is considered for damage analysis (not shown in Fig. 14), the maximum number of tiles crushed at 2.5% drift ratio saturates at 2.

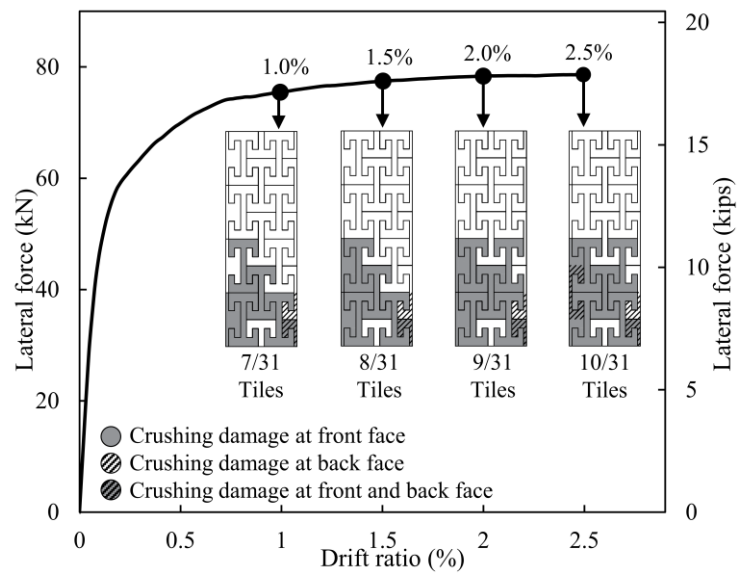


Fig. 14. Damaged tiles due to crushing (unconfined concrete) at varying drift ratios

In addition to results shown in Fig. 13 and Fig. 14, the number of damaged tiles due to cracking and crushing is studied for varying damage thresholds as shown in Fig. 15. These charts show that the number of damaged tiles changes with varying damage thresholds. A tolerable damage threshold can be defined by building owners based on expected performance criteria or by correlating damage in FEA with damage observed in tests to better assess losses. The threshold percentage of cracked elements is varied from 10% through 40%. For crushed elements the threshold is varied between 0% and 1%, i.e., if any or 1% of the finite elements exceeded the strain limit in a tile, the tile was considered damaged.

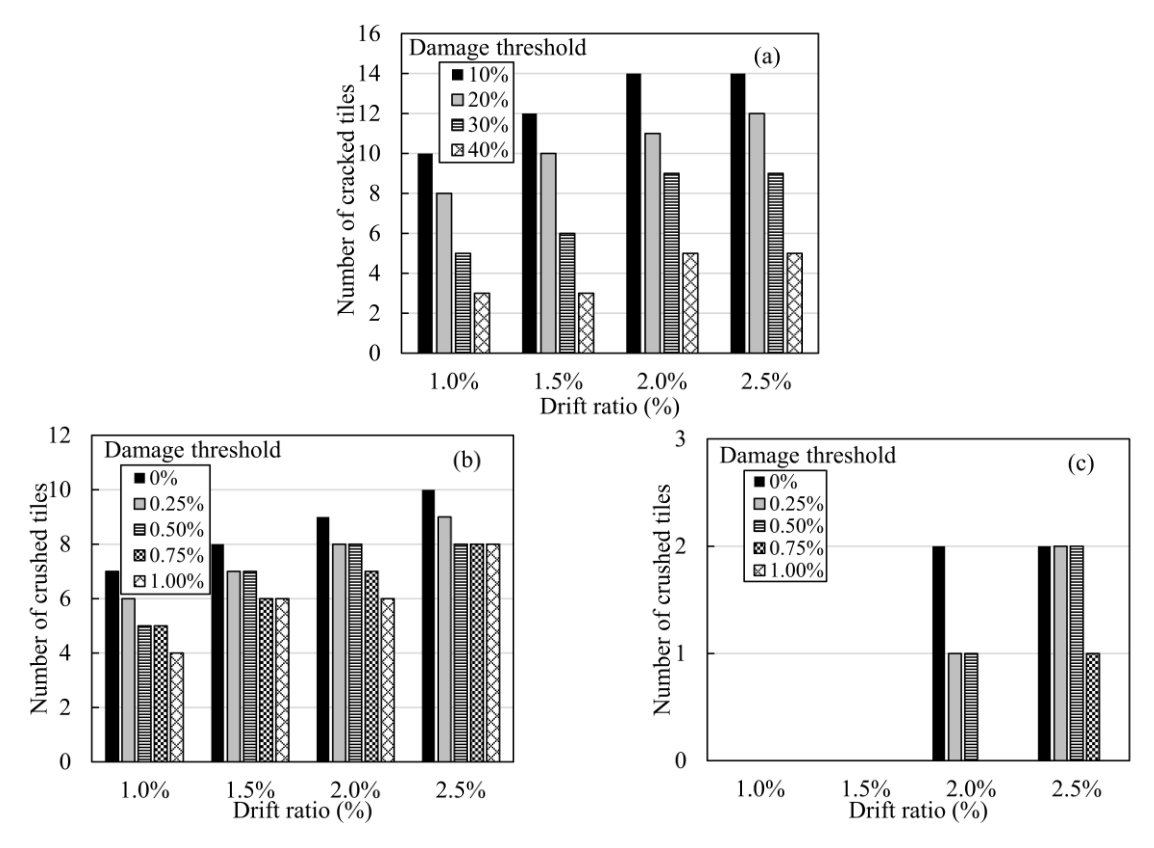


Fig. 15. Number of damaged tiles at varying damage thresholds for (a) Cracking, (b) Crushing (unconfined case) and (c) Crushing (confined case)

7. Parametric Study

The effect of design parameters on the lateral load response of the TeSA wall with staggered pattern B edge tiles is studied, considering the following parameters: 1) concrete strength, 2) friction coefficient between tiles, and 3) reinforcement ratio.

7.1 Concrete Strength

Three concrete compression strength values are considered: 27.6 MPa (4.0 ksi), 43.3 MPa (6.3 ksi, which is the baseline strength) and 55.1 MPa (8.0 ksi). The material models for 27.6 MPa and 55.1 MPa concrete have been taken from the *fib* Model Code 2010 [30]. Fig. 16 (a) shows that increasing concrete strength from 27.6 MPa to 55.1 MPa results in a 7.9% increase in lateral load capacity and 21.5% increase in initial stiffness.

7.2 Friction Coefficient

The baseline model has a friction coefficient of 0.6 between tiles, which is the lower-bound value per ACI 318-14, table 22.9.4.2 [31]. FE analyses are also run for friction coefficient of 1.0 (upper-bound value) to observe its effect on the TeSA wall behavior. A friction coefficient of 1.0 is suggested for "concrete placed against hardened concrete that is clean, free of laitance, and intentionally roughened to a full amplitude of approximately 1/4 in." and friction coefficient of 0.6 is suggested for "concrete placed against hardened concrete that is clean, free of laitance, and not intentionally roughened" by ACI 318-14 [31]. The effect of friction between tiles on the lateral load-displacement behavior of TeSA wall is shown in Fig. 16 (b). The results show that the lateral load capacity of the TeSA wall is virtually independent of the friction coefficient between tiles, with the peak strength changing by less than 1% and the initial stiffness changing by 2.2%. This could be attributed to the gap opening and bearing forces from interlocking, which control the response rather than tangential contact. Gap openings, at relatively small drift ratios, may prevent the development of friction force between tiles.

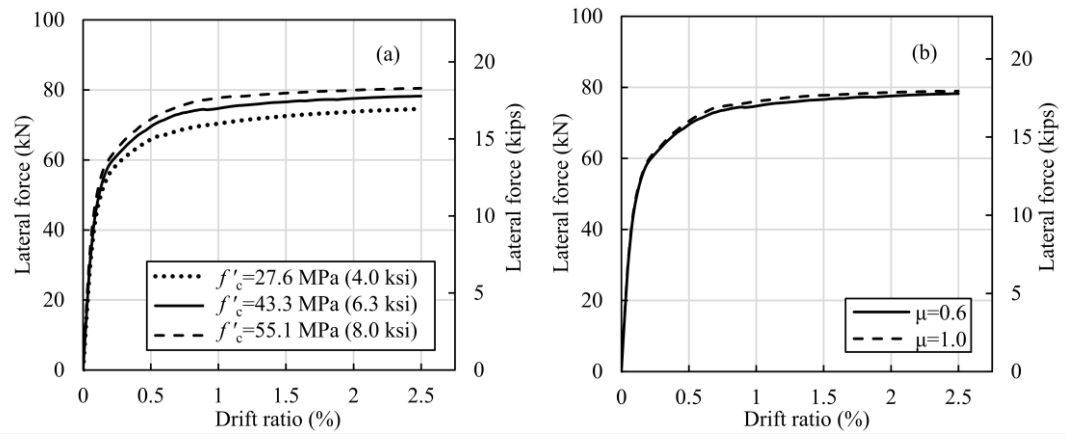


Fig. 16. Effect of (a) concrete strength (b) friction coefficient on the load-displacement response of TeSA wall

7.3 Reinforcement Ratio

The amount of reinforcement in the edge tiles and remainder of the tiles, henceforth referred to as web tiles, is varied to study the effect of reinforcement ratio on the lateral behavior of the TeSA wall. The reinforcement ratios of edge and web tiles for the baseline wall are denoted as ρ_{edge} (1.2%) and ρ_{web} (2.5%), respectively. The reinforcement amount is varied as follows:

- TeSA wall with four times the reinforcement in edge tiles as the baseline TeSA wall ($4\rho_{edge}$ and ρ_{web}),
- TeSA wall with four times the reinforcement in web tiles as the baseline TeSA wall (ρ_{edge} and $4\rho_{web}$),
- TeSA wall with four times the reinforcement in both the edge and web tiles as the baseline TeSA wall
 (4ρ_{edge} and 4ρ_{web}).

The results of the parametric study involving the reinforcement ratios are shown in Fig. 17. Quadrupling the reinforcement area in both the wall edge and wall web increases the lateral load capacity from 78.6 kN (17.7 kips) to 104.0 kN (23.4 kips), a 32.4% increase; and increases the initial stiffness from 17.8 kN/mm (101.6 kip/in) to 20.4 kN/mm (116.5 kip/in), a 15% increase. Quadrupling the reinforcement area, only in the web tiles increases the capacity by approximately 18% and stiffness by 4%, and quadrupling the reinforcement area only in edge tiles increases the capacity by about 8% and increases the stiffness by 10%.

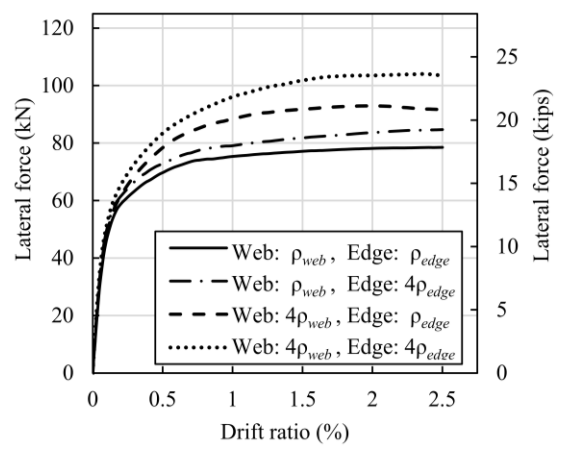


Fig. 17. Effect of doubling the reinforcement bar diameter (quadrupling the bar area) on the lateral load-deformation behavior of TeSA wall

Moreover, it is observed from sectional analysis of conventional walls that an increase in the axial load on the conventional wall increases its capacity when the axial load is below the balance point. This is also expected to be the case for TeSA walls. In addition, axial compression is expected to better control gap opening between tiles for TeSA walls.

7.4 Summary of the Parametric Study Results

Table 1 summarizes the results of the parametric study. The analyses include cases in which different parameters (concrete strength (f'_c) , coefficient of friction between tiles (μ) , and reinforcement ratios (ρ))

are varied simultaneously. For each analysis case, the initial wall stiffness (K) and peak lateral force (V) are provided. These are also expressed as ratios to the values for the baseline case (case 1) as K_i/K_I and V_i/V_I . The parameter that is varied is italicized for each case in Table 1.

Table 1. Parametric study table and FEA result for each case

Case no,	μ	f_c'	ρ_{web}	ρ_{edge}	K	$K_i/K_{i=1}$	V	$V_i/V_{i=1}$
i		MPa (ksi)	%	%	kN/mm (kip/in.)		kN (kip)	
1	0.6	43.3 (6.3)	1.2	2.5	17.8 (101.6)	1.00	78.6 (17.7)	1.00
2	0.6	27.6 (4.0)	1.2	2.5	16.8 (95.9)	0.94	74.8 (16.8)	0.95
3	1.0	43.3 (6.3)	1.2	2.5	18.2 (103.9)	1.02	79.2 (17.8)	1.01
4	0.6	55.1 (8.0)	1.2	2.5	20.4 (116.5)	1.15	80.5 (18.1)	1.02
5	1.0	55.1 (8.0)	1.2	2.5	21.3 (121.6)	1.20	80.6 (18.1)	1.03
6	0.6	43.3 (6.3)	4.8	2.5	18.6 (106.2)	1.04	93.0 (20.9)	1.18
7	0.6	43.3 (6.3)	1.2	10.0	19.6 (111.9)	1.10	84.7 (19.0)	1.08
8	0.6	43.3 (6.3)	4.8	10.0	20.4 (116.5)	1.15	104.0 (23.4)	1.32
9	1.0	43.3 (6.3)	4.8	10.0	21.1 (120.5)	1.19	106.6 (24.0)	1.36
10	1.0	55.1 (8.0)	4.8	10.0	23.8 (135.9)	1.34	110.4 (24.8)	1.40

Lateral strength and stiffness of the TeSA wall are more sensitive to changes in reinforcement area than coefficient of friction between tiles and concrete strength. Additionally, comparing cases 1, 6, and 7 shows that increasing the web reinforcement amount is a more effective way to enhance the lateral load capacity than increasing the edge reinforcement amount.

8. Analytical Method to Estimate Wall Capacity

A simple sectional analysis is carried out to estimate the lower-bound and the upper-bound values of the lateral capacity of TeSA walls governed by flexure. The analysis has the following steps: 1) Unique wall cross-sections across the wall height are identified. 2) These cross sections are analyzed for their lower-bound and upper-bound moment capacities as shown in Fig. 18. Reinforcement is only considered if it is continuous across the cross-section being analyzed. For the lower-bound moment estimate, concrete at discontinuous cross-sections (tile joints) is assumed to carry neither compression nor tension and is neglected. For the upper-bound moment estimate, concrete at discontinuous cross-sections (tile joints) is assumed to transfer compression but not tension. Reinforcement bars and the hatched concrete areas shown in Fig. 18 show the reinforcement and areas of concrete compression resistance considered in moment capacity estimation, respectively. 3) Moment capacity of the wall calculated at various cross sections

through steps 1 and 3 is plotted against the wall height. 4) The moment demand on the wall is plotted across wall height, considering that the demand varies linearly between zero moment at wall top and maximum moment at wall base, for a wall where there is a single lateral load at wall top. 5) Considering that the theoretical demand cannot exceed the capacity without failure, the intersection of the capacity and demand lines is at the point of smallest moment capacity across the wall height. 6) Moment capacity at the base and the maximum lateral load at top of the wall is calculated using geometry for both the lower-bound and the upper-bound cases. This procedure is demonstrated on the TeSA wall with staggered pattern B edge tiles with baseline concrete strength, friction coefficient and reinforcement ratio as an example. The friction coefficient is not used in the analytical method but used in FE models that are used for evaluating the analytical method.

For the TeSA wall with the staggered pattern B edge tiles, three unique cross-sections are identified within the first row of Full tiles from the base. These three cross-sections, labeled as Sections 1-1, 2-2 and 3-3 in Fig. 18, repeat across the wall height. All tiles at section 1-1 are considered to have reinforcement continuous to the foundation. Within the staggered edge tiles, only one of the two edge tiles is continuous across sections 2-2 and 3-3 at each edge.

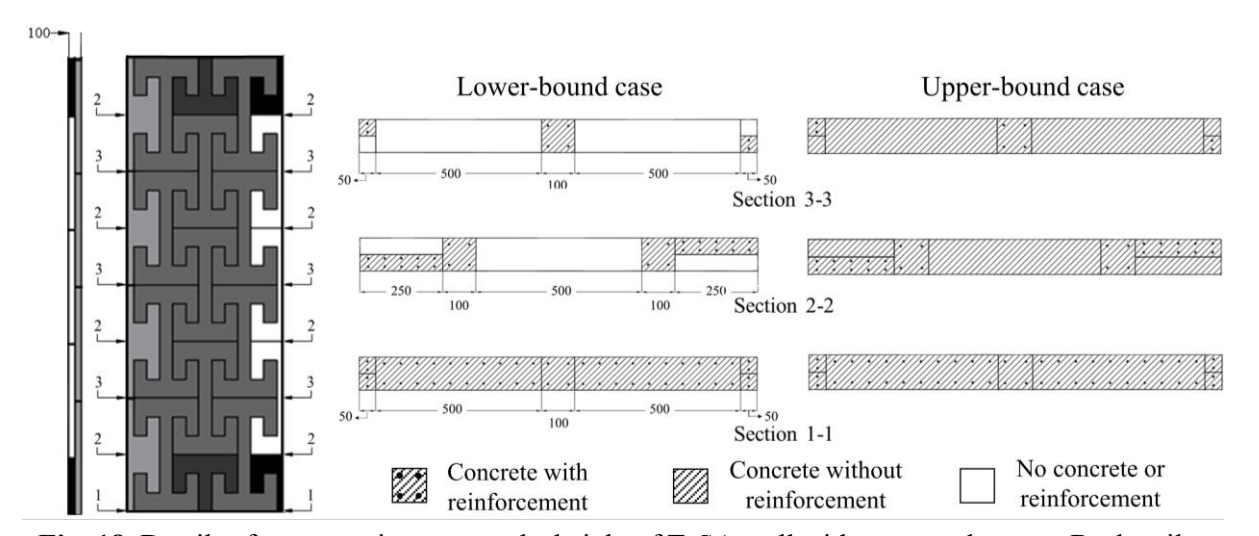


Fig. 18. Details of cross-sections across the height of TeSA wall with staggered pattern B edge tiles

A fiber based cross-sectional analysis is performed to calculate the moment capacity. In fiber based

analyses, the cross-section is discretized into fibers that are assigned the material properties of concrete or

reinforcing steel, depending on the fiber location. Using strain compatibility across the cross-section, the neutral axis location at failure is determined by satisfying section equilibrium. Forces in steel and concrete at failure are calculated and are used to calculate the moment capacity. Concrete and steel constitutive properties are kept the same as that of the FEA model, except that the tensile strength of concrete is assumed to be zero in the simplified analytical model.

Fig. 19 shows the calculated moment capacities along with the demand lines for the lower-bound and the upper-bound cases. The demand line intersects the capacity prediction at the top of Full tiles in the first row (section 3-3) for all cases. The wall is expected to fail at this location. The moment capacities at the wall

base are 105 kN-m (929 kip-in.) and 376 kN-m (3328 kip-in.) for the lower and the upper-bound cases,

respectively, and are calculated from the capacity at section 3-3 using geometry.

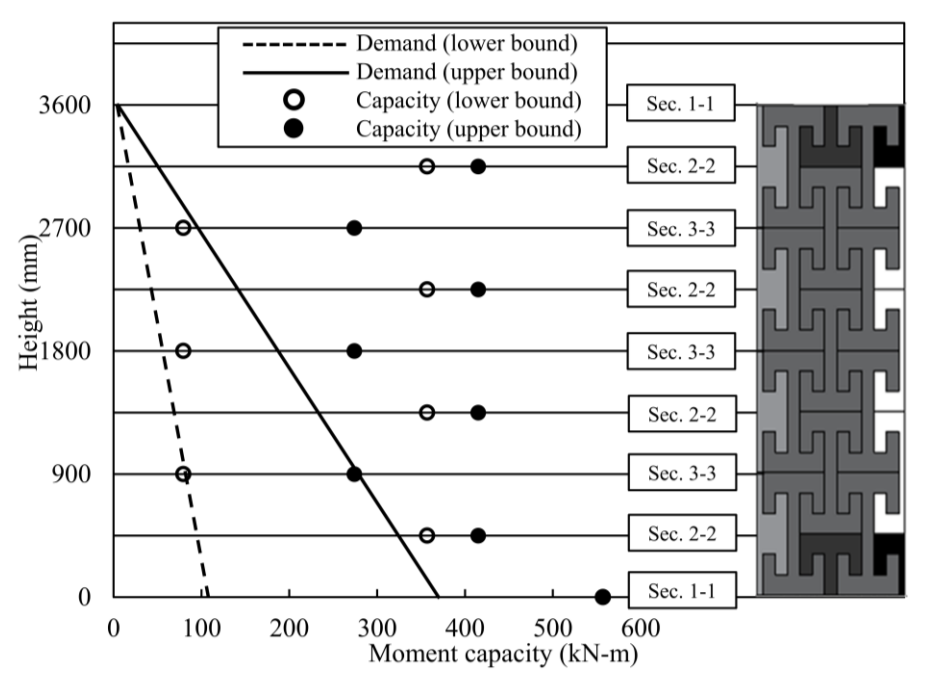


Fig. 19. Moment capacities and demands of TeSA wall sections with staggered pattern B edge tiles Fig. 20 compares the lateral load capacities of walls predicted by the simplified method to the capacities predicted by FEA for the walls analyzed as part of the parametric study (Table 1). All FEA capacity predictions lie within the bounds provided by the simplified-analysis method.

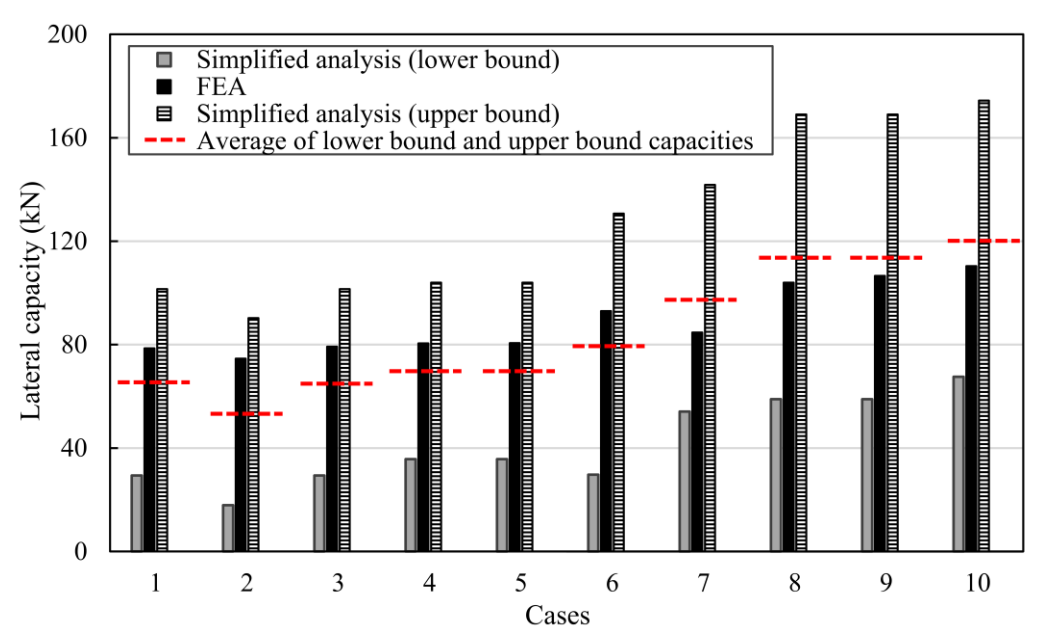


Fig. 20. Lower bound, upper bound and their average values from simplified analysis, and FEA values

For predicting the capacity of TeSA walls from the bounds obtained from the simplified analyses, a method is proposed. The lower-bound capacity estimate (F_{LB}) assumes no concrete contribution at tile joints to capacity. The upper-bound capacity estimate (F_{UB}) assumes full concrete contribution at tile joints to capacity. Thus, the contribution of concrete at tile joints alone to the capacity can be calculated as the difference between the upper and lower-bound estimates, $F_{UB} - F_{LB}$. Fig. 20 shows that FEA predictions are within bounds, indicating that concrete at tile joints may be partially engaged. Therefore, the proposed method involves calculating a weighted sum of the lower-bound estimate (F_{LB}) and the contribution of concrete at tile joints alone ($F_{UB} - F_{LB}$) as shown in equation (1), where (α) and (β) are weights assigned to (F_{LB}) and ($F_{UB} - F_{LB}$), respectively. In this equation, (α) is assigned to be 1 to capture the contribution of continuous reinforcing steel and concrete. The weight of ($F_{UB} - F_{LB}$) is determined by minimizing the root-mean square error in predicting the capacities of each case shown in Table 1.

$$F = \alpha F_{LB} + \beta (F_{UB} - F_{LB}) \tag{1}$$

The resulting equation considering weights obtained after minimizing the prediction error is shown in equation (2):

$$F = 0.48F_{LB} + 0.52F_{UB} \tag{2}$$

The weights so obtained are very close to what simple averaging of the bounds yields. Therefore, averaging of lower and upper-bound estimates can be used for estimating TeSA wall capacity. This average is also shown in Fig. 20. The weighted sum method reasonably estimates capacities for all cases, with the minimum and maximum errors of 9.0% and 25.5% respectively and an average error of 14.1%. If simple averaging is considered, the minimum and maximum errors in prediction are 6.9% and 27.5% respectively, and the average error is 14.4%. The method underestimated capacity for 60% of the cases considered and overestimated it for the remaining 40%.

9. Conclusions

- In this research, an integrated tessellated structural-architectural (TeSA) reinforced concrete (RC) wall system is analyzed as a structural lateral load-resisting system. TeSA walls offer several structural and architectural benefits including modularization, accelerated construction, resiliency and sustainability through contained damage, reparability, deconstructability, and aesthetics. The behavior of TeSA walls with different tile configurations was characterized using the finite element method. The modeling approach was validated using test data on a conventional RC shear wall. The following are the main conclusions:
 - Edge tile configuration had a nominal impact on TeSA wall lateral load capacity and stiffness. TeSA walls with noncontinuous edge tiles had 49% of the lateral load capacity of the equivalent conventional wall. TeSA walls with staggered pattern A, staggered pattern B, and continuous edge tile configurations had 56%, 50% and 51% of the capacity of the conventional wall respectively.
 - TeSA wall with staggered pattern B tiles was studied further to understand damage under lateral load. Damage in the form of concrete cracking and crushing was evaluated considering the percentage of finite elements that exceeded threshold cracking and unconfined crushing strains. The TeSA wall with staggered pattern B edge tiles had considerably less concrete cracking and crushing as compared to the conventional wall. At the ultimate drift ratio of 2.5%, 18.6% and 1.7% of the finite elements cracked and crushed respectively, for the TeSA wall as compared to 27.1%

- and 4.6% of finite elements cracking and crushing, respectively, for the conventional wall. Concrete crushing in both the TeSA wall with staggered pattern B edge tiles and the conventional wall started at a drift ratio of nearly 0.5%. However, crushing did not progress as rapidly in the TeSA wall as it did for the conventional wall at higher drift ratios.
- The number of tiles that would require repair or replacement owing to cracking or crushing was also evaluated at salient drift ratios and varying criteria of damage thresholds. The correlation of strains obtained from FEA with damage observed during testing or in the field can help inform building owners, architects and structural engineers on the expected performance of the TeSA wall by quantifying performance in terms of number of damaged tiles.
- A parametric study was conducted to investigate the effects of concrete strength, coefficient of friction between tiles, and reinforcement ratio in the web and edge tiles on TeSA wall's lateral load-deformation behavior. Doubling the concrete compressive strength resulted in an increase of 7.9% in lateral load and an increase of 21.5% in initial stiffness. Changing the coefficient of friction between tiles had an insignificant effect on lateral load and lateral stiffness (less than 1.0% increase for the former and 2.2% for the latter). Changes in the tile reinforcement ratio had a more prominent effect on the lateral load capacity compared to changes in friction coefficient or concrete strength. It was shown that quadrupling the reinforcement area simultaneously in edge and web tiles increased the lateral load capacity by 32.4%. Quadrupling the reinforcement area in the web tiles only and in the edge tiles only resulted in increase in capacity of 18.0% and 8.0%, respectively. The greater capacity gain by the increase of reinforcement in the web tiles was due to the fact that web tiles took up a major part of the wall cross section.
- TeSA walls, in general, had smaller capacities as compared to equivalent conventional walls. To
 obtain similar strength with TeSA walls, additional reinforcement, larger shear walls or additional
 shear walls may be necessary. Architectural opportunities offered by TeSA walls may provide
 incentive to offset the cost of additional reinforcement and/or walls.

• A simple cross-section equilibrium based analysis approach, which predicts the lower and upper bounds of the TeSA wall capacity by identifying unique cross sections across wall height, was proposed. A method for estimating the capacity of TeSA walls using the calculated bounds from sectional analysis was also outlined. When the lower-bound and upper-bound estimates obtained using the simple analysis approach were averaged, this average was within 25.5% of the capacity estimate obtained from FEA for all cases, with an average error of 14.1% for all cases.

Acknowledgments

- This material is based upon work supported by the National Science Foundation under Grants Nos. 1762133
- and 1762899. Any opinions, findings, and conclusions or recommendations expressed in this material are
- 484 those of the authors and do not necessarily reflect the views of the National Science Foundation.

485 References

475

476

477

478

479

480

- 486 [1] Kuang J, Ho Y. Seismic behavior and ductility of squat reinforced concrete shear walls with nonseismic
- detailing. ACI Structural Journal. 2008;105:225.
- 488 [2] Paulay T. The design of ductile reinforced concrete structural walls for earthquake resistance.
- 489 Earthquake Spectra. 1986;2:783-823.
- 490 [3] Mander JB, Cheng C-T. Seismic resistance of bridge piers based on damage avoidance design.
- 491 Technical Rep No NCEER-97-0014, National Center for Earthquake Engineering Research, . State
- 492 University of New York, Buffalo, NY1997.
- 493 [4] Kurama Y, Sause R, Pessiki S, Lu L-W. Lateral load behavior and seismic design of unbonded post-
- tensioned precast concrete walls. ACI Structural Journal. 1999;96:622-32.
- 495 [5] Priestley MJN, Sritharan S, Conley JR, Pampanin S. Preliminary results and conclusions from the
- 496 PRESSS five-story precast concrete test building. PCI Journal. 1999;44:42-67.
- 497 [6] Holden T, Restrepo J, Mander JB. Seismic performance of precast reinforced and prestressed concrete
- walls. Journal of Structural Engineering. 2003;129:286-96.

- 499 [7] Pampanin S. Emerging solutions for high seismic performance of precast/prestressed concrete buildings.
- Journal of Advanced Concrete Technology. 2005;3:207-23.
- [8] Restrepo JI, Rahman A. Seismic performance of self-centering structural walls incorporating energy
- dissipators. Journal of Structural Engineering. 2007;133:1560-70.
- 503 [9] Hamid N, Mander JB. Lateral seismic performance of multipanel precast hollowcore walls. Journal of
- 504 Structural Engineering. 2010;136:795-804.
- 505 [10] Sritharan S, Aaleti S, Henry RS, Liu KY, Tsai KC. Precast concrete wall with end columns (PreWEC)
- for earthquake resistant design. Earthquake Engineering & Structural Dynamics. 2015;44:2075-92.
- 507 [11] Yang C, Okumus P. Ultrahigh-performance concrete for posttensioned precast bridge piers for seismic
- resilience. Journal of Structural Engineering. 2017;143:04017161.
- 509 [12] Basereh S, Okumus P, Aaleti S. Reinforced-concrete shear walls retrofitted using weakening and self-
- 510 centering: Numerical modeling. Journal of Structural Engineering. 2020;146:04020122.
- [13] Wallace JW. Behavior, design, and modeling of structural walls and coupling beams Lessons from
- 512 recent laboratory tests and earthquakes. International Journal of Concrete Structures and Materials.
- 513 2012;6:3-18.
- 514 [14] Birely AC. Seismic performance of slender reinforced concrete structural walls [Doctoral dissertation]:
- 515 University of Washington; 2012.
- 516 [15] Ross BE, Yang C, Kleiss MCB, Okumus P, Khorasani NE. Tessellated structural-architectural
- 517 systems: Concept for efficient construction, repair, and disassembly. Journal of Architectural Engineering.
- 518 2020;26:04020020.
- 519 [16] Moore D. The Roman Pantheon: The triumph of concrete: MARC/CCEOP, University of Guam
- 520 Station; 1995.
- 521 [17] Molotnikov A, Estrin Y, Dyskin A, Pasternak E, Kanel-Belov A. Percolation mechanism of failure of
- a planar assembly of interlocked osteomorphic elements. Engineering Fracture Mechanics. 2007;74:1222-
- 523 32.

- 524 [18] Estrin Y, Dyskin A, Pasternak E, Schaare S, Stanchits S, Kanel-Belov A. Negative stiffness of a layer
- with topologically interlocked elements. Scripta Materialia. 2004;50:291-4.
- 526 [19] Mather A, Cipra R, Siegmund T. Structural integrity during remanufacture of a topologically
- 527 interlocked material. International Journal of Structural Integrity. 2012;3:61-78.
- 528 [20] Zareiyan B, Khoshnevis B. Effects of interlocking on interlayer adhesion and strength of structures in
- 3D printing of concrete. Automation in Construction. 2017;83:212-21.
- 530 [21] Javan AR, Seifi H, Xu S, Ruan D, Xie Y. The impact behaviour of plate-like assemblies made of new
- interlocking bricks: An experimental study. Materials & Design. 2017;134:361-73.
- 532 [22] Brugger C, Fivel MC, Brechet Y. Numerical simulations of topologically interlocked materials
- 533 coupling DEM methods and FEM calculations: Comparison with indentation experiments. MRS Online
- Proceedings Library Archive. 2009;1188.
- 535 [23] Thomsen JH, Wallace JW. Displacement-based design of slender reinforced concrete structural walls
- Experimental verification. Journal of Structural Engineering. 2004;130:618-30.
- 537 [24] Abaqus. Abaqus analysis user's manual, 6.16-1. Providence, RI, USA. 2016.
- 538 [25] Thomsen JH, Wallace JW. Displacement-based design of reinforced concrete structural walls:
- Experimental studies of walls with rectangular and T-shaped cross sections. Rep. No. CU/CEE-95/06:
- 540 Clarkson University, N.Y.; 1995.
- 541 [26] Lubliner J, Oliver J, Oller S, Oñate E. A plastic-damage model for concrete. International Journal of
- 542 Solids and Structures. 1989;25:299-326.
- 543 [27] Lee J, Fenves GL. Plastic-damage model for cyclic loading of concrete structures. Journal of
- 544 Engineering Mechanics. 1998;124:892-900.
- 545 [28] Lim JC, Ozbakkaloglu T, Gholampour A, Bennett T, Sadeghi R. Finite-element modeling of actively
- confined normal-strength and high-strength concrete under uniaxial, biaxial, and triaxial compression.
- Journal of Structural Engineering. 2016;142:04016113.

- 548 [29] Wosatko A, Winnicki A, Polak MA, Pamin J. Role of dilatancy angle in plasticity-based models of
- concrete. Archives of Civil and Mechanical Engineering. 2019;19:1268-83.
- 550 [30] fib. FIB model code for concrete structures 2010. Lausanne, Switzerland: Fédération Internationale du
- 551 Béton (FIB). 2010.
- 552 [31] ACI. Building code requirements for structural concrete (ACI 318-14) and commentary (318 R-14).
- 553 Farmington Hills, MI: ACI. 2014.
- 554 [32] Mander JB, Priestley MJ, Park R. Theoretical stress-strain model for confined concrete. Journal of
- 555 Structural Engineering. 1988;114:1804-26.
- 556 [33] Karthik MM, Mander JB. Stress-block parameters for unconfined and confined concrete based on a
- unified stress-strain model. Journal of Structural Engineering. 2011;137:270-3.